Semiempirical Characterization of Homonuclear Diatomic Ions: 6. Group VI and VII Anions

Edward S. Chen*,† and Edward C. M. Chen‡

Center for High Performance Software, Rice University, Houston, Texas 77005, and University of Houston Clear Lake, 4039 Drummond, Houston, Texas 77025

Received: September 2, 2002; In Final Form: October 27, 2002

Sixteen Herschbach ionic Morse potential energy curves (HIMPEC) were classified using molecular ion formation M or dissociation D in a vertical transition. Two activation energies for thermal electron attachment to Cl_2, Br_2, and I_2 are reported from a reanalysis of electron-capture detector data. The HIMPEC for the diatomic halogens and oxygen are optimized by including new experimental data. All of the halogen curves are defined by at least three data points. Two new curves for the $^2\Pi_g(1/2)$ states of $Br_2(-)$ and $I_2(-)$ are constructed using a lower experimental dissociation energy. New electron-capture detector data for O_2 confirm multiple activation energies and electron affinities, E_a. The twelve M and twelve D curves for the 24 predicted anionic states of O_2 are calculated using E_a, vertical electron affinities, activation energies, frequencies, and estimated dissociation energies. Two curves are calculated from experimental data for anions of S_2, Se_2, and Te_2.

Introduction

This series characterizes homonuclear diatomic ions using Morse potential energy curves, MPEC. Curves were calculated for the rare-gas positive ions, $Rg_2(+)$ in part 4 and $H_2(-)$, $O_2(-)$, and the halogen anions $X_2(-)$ in part 5.[1,2] The latter were used to illustrate eight primary and eight secondary Herschbach ionic Morse potential energy curves, HIMPEC. These were based on Molecular anion formation or Dissociation in a vertical electron transition and the sign of three metrics: the electron affinities, E_a, the vertical electron affinities, VE_a, and the energy for dissociative electron attachment, $E_{dea} = E_a(X) - BDE$.[1,3] The E_a are positive for exothermic reactions, and BDE is the bond dissociation energy. The curves are M(m), D(m), Mc(m), and Dc(m) for $m = 0$ to 3, where m is the number of positive metrics and Mc and Dc refer to crossings with the polarization curves. The VE_a are the energy differences between the anion and neutral in the geometry of the ground-state neutral. The E_a are the energy differences for the most stable form of each anionic state and the ground-state neutral. The largest E_a or adiabatic E_a, AE_a is positive. The Herschbach metrics give two points on the Morse potentials. The electron-impact distribution or activation energy for electron attachment, E_1 gives a third point. The experimental data in the region of the internuclear separation of the neutral, r_e, are more easily visualized by using $S = 1 - (r/r_e)$, the modified Simons, Parr, and Finlan variable.[4]

Ground-state HIMPEC for the main-group homonuclear anions are now well defined, but few excited-state curves are available. Improved curves for $X_2(-)$, 24 curves for $O_2(-)$, and 2 anionic curves for S_2, Se_2, and Te_2 are constructed. The experimental characterization of anionic states is important for theoretical calculations. Multiple states of $O_2(-)$ are important to atmospheric and biological processes.

AE_a values of X_2 determined from photoelectron spectroscopy, PES, alkali-metal beam (AMB), charge-transfer complex (CTC), ion beam (IB), and electron-impact (EI) data agree within the uncertainties. The weighted-average values are F_2, 3.05 ± 0.08 eV; Cl_2, 2.45 ± 0.15 eV; Br_2, 2.56 ± 0.05 eV; and I_2, 2.524 ± 0.005 eV.[5−7] All data not specifically cited come from available compilations.[5] These are supported by the experimental dissociation energies of the isoelectronic rare-gas positive ions, $D_0(X_2(-)) = D_0(Rg_2(+))$. A BDE (0.015 eV) for the $^2\Pi_g(1/2)$ state of $I_2(-)$ has been measured using PES.[8] New data for excited states of $Ar_2(+)$ have been published.[9] The reanalysis of electron-capture detector (ECD) data for Cl_2, Br_2, and I_2 gives two activation energies E_1 from $k_1 = A_1T^{-1/2}\exp(-E_1/RT)$. Updated HIMPEC for $X_2(-)$ will incorporate these data with earlier data.[10−16]

The superoxide anion was the first homonuclear diatomic anion observed, and a large body of data has been produced from different experimental and theoretical studies, some of which is unexplained.[17−33] Experimental data for two anionic states of S_2, Se_2, and Te_2 are available.[34−37] From a 1953 review, the AE_a of O_2 was 0.9 eV, and the low-energy electron attachment leads to an excited state.[17] Values now range from 0.15 to 1.07 eV: (method, E_a(eV), dates)—photodetachment, PD 0.1_5, 1958; CTC, 0.7_5, 1961−1971; electron swarm, 0.4_5, 1961; EB, 0.6, $1._1$, 1961−1971; AMB, 0.2, 0.3, 0.5, 0.8, $1._3$, 1970−1977; IB, 1.0_7, 1970; PES, 0.43, 0.45, 1971−1995; and ECD, 0.4_5, 0.5, 0.9, 1970−2002.[5,18−25] The range of the values indicates systematic differences. The experimental VE_a range from 0.9 to −17 eV.[26−32]

The electron swarm and the ECD methods give absolute E_a by measuring K_{eq} for thermal electron reactions as a function of temperature. The slope of a plot of $\ln(K_{eq}T^{3/2})$ versus $1000/T$ is E_a/R, giving the E_a from the data and R. The complete temperature dependence for a given state in the ECD is determined by four parameters: E_a, Q_{an} (the partition function ratio for the anion and neutral excluding spin multiplicity), A_1, and E_1. Two or more anionic states have been identified in the

* Corresponding author. E-mail: echen@rice.edu.
† Rice University.
‡ University of Houston.

10.1021/jp0268922 CCC: $25.00
Published on Web 12/10/2002

ECD data for O_2, NO, CS_2, chloroethylenes, halobenzenes, and aromatic hydrocarbons.[21−23,38−40] These quantities have also been determined using negative-ion mass spectrometry.[41−43] New ECD data identifying multiple low-lying anionic states for O_2 will be compared with published data.

Bates and Massey proposed four bound $O_2(-)$ states leading to $O(^3P_g) + O(-)^2P_u$.[44] Gilmore identified 24 states: $[^2\Sigma_g^-(2)$, $^2\Sigma_u^-(2)$, $^4\Sigma_g^-(2)$, $^4\Sigma_u^-(2)$, $^2\Sigma_g^+$, $^2\Sigma_u^+$, $^4\Sigma_g^+$, $^4\Sigma_u^+$; $^2\Pi_g(2)$, $^2\Pi_u(2)$, $^4\Pi_g(2)$, $^4\Pi_u(2)$, and $^2\Delta_g$, $^2\Delta_u$, $^4\Delta_g$, $^4\Delta_u]$.[45] In 1981, Michels calculated curves for these states and E_a that range from −1.5 to −3.7 eV for 11 bound excited states of $O_2(-)$.[46] Four curves have been constructed: the $(3\sigma_g)^2$, $(1\pi_u)$,[4] $(1\pi_g)^3$, and $(3\sigma_u)^0$ 2430 $^2\Pi_g$ ground state, A$E_a = 1.0_7$ eV; the $^4\Sigma$ state, $E_a = 0.9$ eV; the 2340 $^2\Pi_u$ state, $E_a = 0.43$, 0.45 ± 0.002 eV; and the 1431 or 1341 $^2\Pi$ state, $E_a = -2.8$ eV.[1,26,31] As proposed in part 5, 12 M and 12 D HIMPEC are calculated for the predicted 24 states by assigning the experimental and theoretical E_a and VE_a. These are compared with published curves.

Morse Potential Energy Curves

The Morse potentials for the neutral and the HIMPEC as referenced to zero energy at infinite separation are

$$U(X_2) = -2D_e(X_2)\exp(-\beta(r - r_e)) + 2D_e(X_2)\exp(-2\beta(r - r_e)) \quad (1)$$

$$U(X_2^-) = -2k_A D_e(X_2)\exp(-k_B\beta(r - r_e)) + k_R D_e(X_2)\exp(-2k_B\beta(r - r_e)) - E_a(X) + E(X^*) \quad (2)$$

where r is the internuclear separation, $E(X^*)$ is the spin−orbit excitation energy of the atom, $D_e(X_2)$ is the spectroscopic dissociation energy of the neutral, $\beta(X_2) = \nu_e(2\pi^2\mu/D_e)^{1/2}$, μ is the reduced mass of the neutral, ν_e is the frequency of the neutral, and $r_e = r$ at the minimum of $U(X_2)$. k_A, k_B, and k_R are dimensionless constants. Equation 2 is written in terms of the Morse parameters of the neutral. However, it is also a Morse potential. By using $k_B = \beta(X_2^-)/\beta(X_2)$ and the standard form of the Morse potential for the HIMPEC, the following equations for the ionic Morse parameters can be obtained:

$$D_e(X_2^-) = [k_A^2/k_R]D_e(X_2) \quad (3)$$

$$r_e(X_2^-) = [\ln(k_R/k_A)]/[k_B\beta(X_2)] + r_e(X_2) \quad (4)$$

$$\upsilon_e(X_2^-) = [k_A k_B/k_R^{1/2}]\upsilon_e(X_2) \quad (5)$$

$$-VE_a = (1 - 2k_A + k_R)D_e(X_2) - E_a(X) + E(X^*) - {}^1/_2 h\upsilon_e(X_2) \quad (6)$$

The Herschbach metrics E_{dea}, E_a, and VE_a give k_A and k_R using eqs 3 and 6. A value of the frequency or r_e gives k_B from eq 4 or 5 to define the HIMPEC. The reduced mass of the ion will be different from that of the neutral. This variation is incorporated into the value of k_B.

Kinetic Model and Data for the Electron-Capture Detector

The ECD is used to study thermal electron reactions at different temperatures.[21−23,38−40] Electrons are rapidly thermalized at atmospheric pressure. The electron current with and without AB, I_{e-} and I_b, are recorded as a sample elutes from the chromatographic column. K[AB] = $\{I_b - I_{e-}\}/2I_e$ is calculated from the amount of sample and the flow rate to give concentration [AB]. The reactions are electron attachment, detachment, dissociation, and recombination with ions, P(+).

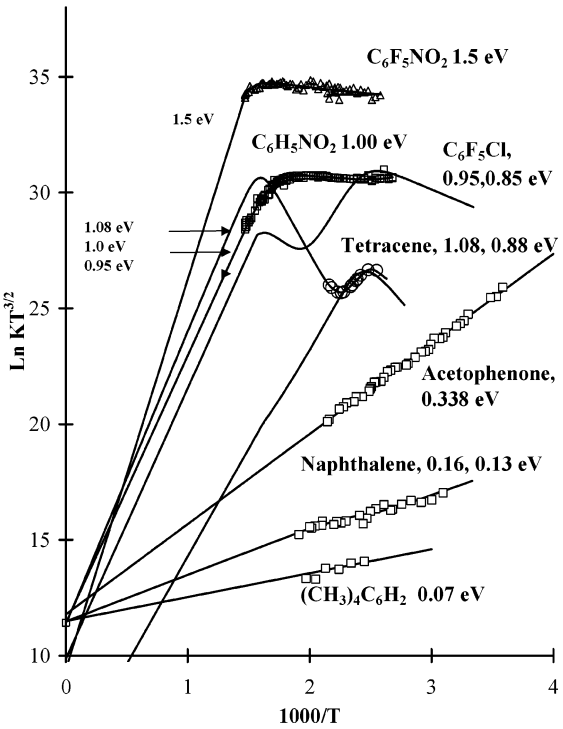

Figure 1. Plot of the molar response of the electron-capture detector as $\ln(KT^{3/2})$ vs $1000/T$. $\ln(k_N/k_D) = 0$.

$$AB + e^- \underset{k_1}{\overset{k_{-1}}{\rightleftharpoons}} AB^- \xrightarrow{k_2} A + B^- \quad (7)$$

$$e^- \text{ or } AB^- + P(+) \xrightarrow{k_D \text{ or } k_N} \text{neutrals} \quad (8)$$

The steady-state treatment for a single state gives

$$K = \frac{k_1(k_N + k_2)}{k_D(k_{-1} + k_N + k_2)} \quad (9)$$

With $k_1 = A_1T^{-1/2}\exp(-E_1/RT)$, $k_{-1} = A_{-1}T\exp(-E_{-1}/RT)$, and $E_a = E_{-1} - E_1$ for more than one state,

$$KT^{3/2} = \sum \frac{(k_N + k_{2i})\{(A_1/A_{-1})_i \exp(E_{ai}/RT)\}}{k_D(1 + k_N/k_{-1i} + k_{2i}/k_{-1i})} \quad (10)$$

When $k_{-1} \gg k_N > k_2$, E_a and Q are determined since

$$\ln KT^{3/2} = \ln[Q] + 12.46 + E_a/RT + \ln(k_N/2k_D) \quad (11)$$

The value of 12.46 is calculated from fundamental constants, and the translational partition function of the electron and $\ln(k_N/2k_D)$ are instrumental constants.

When $k_{-1} \ll (k_N + k_2)$, A_1 and E_1 are determined since

$$\ln KT^{3/2} = \ln[A_1T/k_D] - E_1/RT \quad (12)$$

$A_{1(max)}$ ($E_1 = 0$) is the de Broglie A_1, DeBA. The value of ln(DeBA) calculated from fundamental constants is about 36.

In Figure 1, ECD data are presented as $\ln KT^{3/2}$ versus $1000/T$ for several organic molecules. In Figures 2 and 3 are ECD data for X_2 and O_2. The X_2 data and the details of the experimental procedures have been previously published.[15] The 1972 data for O_2 in Figure 2 were published by other investigators. The

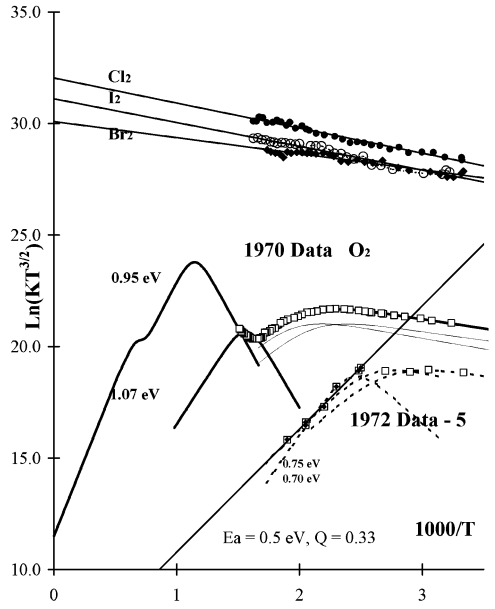

Figure 2. Molar response of the electron-capture detector as $\ln(KT^{3/2})$ vs $1000/T$ for X_2 and O_2. 1970 data, refs 21 and 22; 1972 data, displaced down by 5 units, ref 23.

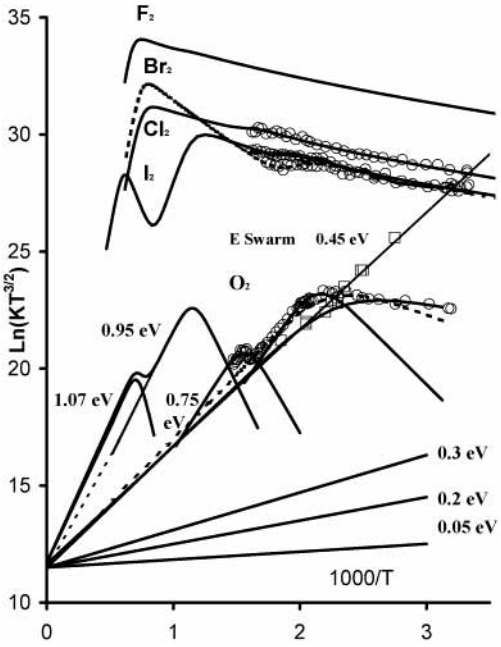

Figure 3. Plot of the molar response of the electron-capture detector as $\ln(KT^{3/2})$ vs $1000/T$. New O_2 data were obtained as follows: extra-dry 99.6% O_2 was introduced into a porapak Q column at room temperature with a gas-sampling valve. The detector temperature was elevated to 673 K, and measurements were made at subsequently stabilized lower temperatures. The data were obtained with a high-temperature tritium source and purified Ar−10% CH_4.

1970 ECD data were originally published only in a dissertation.[21] Also in Figure 3 are electron swarm and new ECD data for O_2.[19] The experimental conditions for the ECD data are shown in the caption. The parameters used to obtain the curves are given in Table 1.

The data in Figure 1 illustrate the determination of E_a, Q, A_1, and E_1. The highest measured E_a is 1.5 eV for $C_6F_5NO_2$, the lowest, 0.07 ± 0.02 eV for tetramethylbenzene, and the most precise, 0.338 ± 0.002 eV for acetophenone. For tetracene, naphthalene, and C_6F_5Cl, two states are observed, and eight quantities are calculated. More than two states have been

TABLE 1: Electron-Capture Detector Data[a]

species	$\ln(A_1)$	E_1 (eV)	Q	E_a (eV)
$C_6F_5NO_2$	36.5	0.01	(0.8)	1.5 ± 0.1
$C_6H_5NO_2$	(32.6)	(0.0)	(1)	1.0 ± 0.01
acetophenone			1	0.338 ± 0.002
$(CH_3)_4C_6H_2$			1	0.07 ± 0.05
C_6F_5Cl	(36.4)	0.4	(1)	0.9_5
C_6F_5Cl	(36.4)	(0.15)	(1)	0.8_5
tetracene	(37)	0.9_5	(1)	1.1 ± 0.05
tetracene	(36)	0.8	10^{-4}	0.88 ± 0.05
naphthalene	(34.2)	0.2	(1)	0.1_3
naphthalene	(33.8)	0.6	(0.8)	0.1_5
F_2	(35.5)	(0.05)	(1)	(3.0_5)
F_2	(33)	(0.03)	(1)	(1.7)
Cl_2	(33)	0.06	(1)	(2.4_5)
Cl_2	(35.5)	0.30	(1)	(1.1)
Br_2	(35.5)	0.28	(1)	(2.5_6)
Br_2	(33)	0.03	(1)	(1.4)
I_2	(35.5)	0.45	(1)	(2.5_2)
I_2	(33)	0.05	(1)	(1.5)
O_2	(24.9)	(0.05)	(1)	(0.45)
	(24.9)	(0.05)	(0.5)	(0.43)
	(24.9)	0.1	(0.8)	(0.5)
	(34.7)	0.4	0.01	0.7
	(35.2)	0.8	0.02	0.7_5
	(35.5)	0.9	(0.8)	(0.9_5)
	(35.5)	(1.9)	(0.8)	(1.0_7)

[a] Values in parentheses are experimental values from other methods or have been estimated.

observed for aromatic hydrocarbons corresponding to the different C−H bonds.[38−40] In 1966, the AE_a of tetracene was determined to be 0.88 rather than 1.1 eV because only one state was considered.[39] Now that the AE_a of tetracene has been measured definitively, the lower value can be assigned to an excited state, and the upturn can be used to obtain a ground-state activation energy. The activation energy to the excited state can be determined by assuming a value for A_1, as shown in Table 1. The large activation energies and the low intercept for the excited state for tetracene obtained from data published by other investigators have not been measured by other techniques. The AE_a of nitrobenzene and tetracene have been confirmed by PES, thermal charge transfer, reduction potentials, and theoretical calculations whereas that of nitrobenzene has also been confirmed by the temperature dependence of the parent negative ion. Molecular anions of $C_6F_5NO_2$, C_6F_5Cl, $C_6H_5NO_2$, tetracene, and O_2 are observed at the highest ECD temperature.[40−43]

Two parameters were obtained for Cl_2, I_2, and Br_2 by considering only one state. The values of these parameters are $\ln(A_1) = 32$, 31, and 30 and $E_1 = 0.1$, 0.09, and 0.06 eV, respectively.[15] In Figure 3, the X_2 curves are calculated with two states and eq 10. The partition function ratios Q were fixed to unity, A_1 values were estimated from linear plots, and the DeBA and the established E_a were used to determine two E_1 values by an iterative nonlinear least-squares procedure. For F_2, the two activation energies were also estimated to be less than the E_1 for Cl_2. Although no ECD data are available, this predicts a higher ECD response and the lower temperature dependence observed in other electron-attachment studies.[16] The activation energies for the attachment to the ground states increase from 0.06 eV for Cl_2 to 0.45 eV for I_2. The calculated backside curve crossings could lead to the formation of molecular anions as observed in AMB studies.

A Q of 0.33 and an E_a of 0.5 ± 0.1 eV were reported for O_2 from the 1972 data.[23] This line is shown in Figure 2. If multiple states are considered, then the deviations are reduced, and electron affinities of 0.7 and 0.75 eV are supported as shown

TABLE 2: Morse Parameters for the Ground State ($X_2(-)$)

	D_o (eV)	r_e (pm)	υ (cm^{-1})	AE_a (eV)	sources
F_2^-	1.28(5)	181(5)	510(30)	3.08(5)	tw
	1.23	192	462	3.0	1985-10
	1.21(10)	179(2)	580(30)	3.08	AMB-7
		189	510	3.05(8)	NIST-5
Cl_2^-	1.32(2)	256(5)	255(4)	2.45(2)	tw
	1.35	262	249	2.46	1985-10
	1.30(15)		255(9)	2.4	AMB-7
Br_2^-	1.18(2)	283(5)	160(4)	2.56(2)	tw
	1.20	285	158	2.57	1985-10
	1.15(10)		160(5)	2.6	AMB-7
I_2^-	1.01(1)	321(0.5)	110(2)	2.52(1)	tw
	1.01(1)	321(0.5)	111(2)	2.52(1)	tw
	1.07	323	113	2.57	1985-10
	1.02(5)		109	2.55	AMB-7
	1.01(1)	321(0.5)	110(2)	2.524(5)	PES-6

by the dotted lines. The temperature dependence of the low-temperature 1970 data could be reproduced from electron swarm data: ln(A_1), 23.7 ± 0.3; E_1, 0.07 ± 0.05 eV; E_a, 0.46 ± 0.05 eV, and Q, 0.5. The high-temperature data defined a second state with $E_a = 1 \pm 0.25$ eV assuming $Q = 1$ with kinetic parameters of ln(A_1) = 39 ± 4 and $E_1 = 1.1 \pm 0.2$ eV. Four parameters for both states have now been measured. These are more precise than the above values but agree with them within the uncertainties.[19,20,24,33] Two spin−orbit coupling states have been resolved by PES.[24] In Figure 2, the calculated ECD curves for these states, separated by 0.02 eV, are shown. When these are combined, they give the curve that is drawn through the data with a reduction in the deviations when compared to only one low-temperature state.[22]

In the new ECD data, besides the initial upturn at higher temperatures, there is a downturn indicative of two additional excited states with E_a of 0.75 and 0.70 eV. In Figure 2, the curves calculated from the new data blend with the 1970 and 1972 data. The E_1, A_1, and Q values are determined from the ECD data for O_2 since the E_a and their uncertainties are used in the data analysis. Since the data analysis cannot degrade the quality of a value, the E_a determined from the ECD data are equally as certain as the independently determined values. The ground-state curve with $E_a = 1.07 \pm 0.07$ eV is calculated from estimates of A_1 and Q and the measured E_1 of 1.9 ± 0.2 eV.[33] The general increase in the activation energy with E_a is characteristic of the inverted Marcus region. Calculated curves for O_2 with E_a of 0.3, 0.2, and 0.05 eV and $Q = 1$ indicate their negligible ECD response.

Calculations of HIMPEC for X_2

In the 1960s, Herschbach estimated six Morse potentials for $I_2(-)$. These curves did not cross and reflected the available experimental E_1, E_a, VE_a, and anion absorption peak energy E(abs). The systematic variation in the E(abs) for the remaining $X_2(-)$ was noted. [3] In 1985, six curves for all of the X_2 were obtained from updated values, electron impact spectra, and E_1. There were no EI data for the two highest states of $I_2(-)$.[10]

In Table 2, the optimum Morse parameters for the ground states of $X_2(-)$ are compared with the 1985 values, the literature, AMB, and PES values. The $I_2(-)$ parameters were determined using PES. The internuclear distances for $Cl_2(-)$ and $Br_2(-)$ are determined from the VE_a. The dissociation energies are defined from both the AE_a and the $Rg_2(+)$ values. The frequencies are measured in solids. The E_1 values from the ECD and the anion absorption spectra support these Morse parameters.

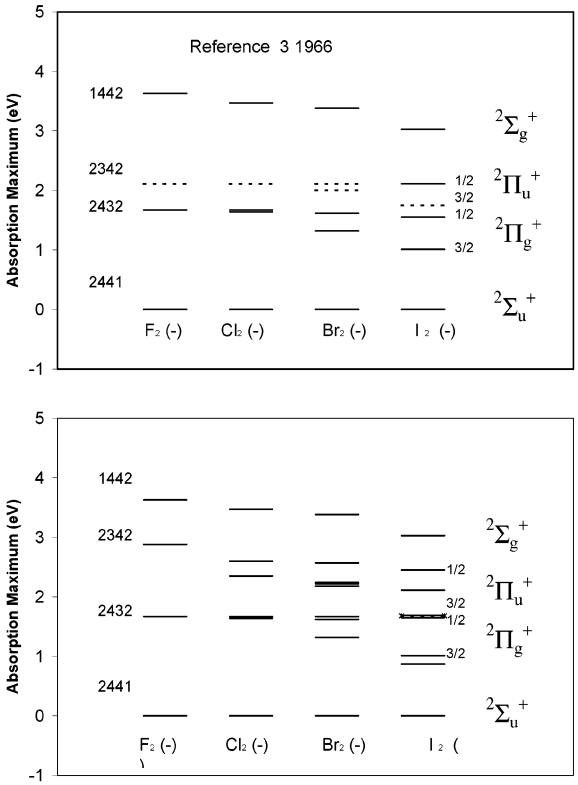

Figure 4. Calculated and experimental anion absorbance maximum from ref 3 and this work. Energies indicated by the dotted lines were estimated from periodic trends in the 1960s. Energies from this work are obtained from the data given in Table 3.

The dissociation energy determined from the experimental AE_a for $F_2(-)$ is 3 meV lower than the value for $Ne_2(+)$. The internuclear distance is larger than the AMB value but smaller than the NIST value. The frequency is the NIST value with the AMB random uncertainty. There are no ECD data for F_2, but other studies give a low E_1 as shown in Table 1.[16] The random uncertainties are estimated from the values given for the experimental quantities or the range of values in Table 2. The systematic uncertainties should be smaller than the random uncertainties, making these values both precise and accurate.

With accurate ground-state curves, it is possible to obtain excited-state curves from the D_o, the VE_a, and one other point—the electron impact ion distribution, the E(abs), or E_1. The experimental D_o of the $Rg_2(+)$ are used for most of the states. The lower D_o for $I_2(-)$ is used for the $^2\Pi_{g1/2}$ curves. Two analogous curves for $Br_2(-)$ are calculated. The calculated and experimental ion distributions are shown in Figure 5, and the optimum Morse curves are shown in Figure 6. The dimensionless constants, the parameters, and the data used to calculate these curves are given in Table 3.

The first step in calculating the curves is to choose the E_a or, equivalently, the D_o. Then the electron-impact distribution is calculated and fit to the experimental data as shown in Figure 5. Two peaks are observed in the highest peak for $Cl_2(-)$, which could be due to another excited state. [10−15] The curves are then fit to the measured E(abs) maxima shown in bold in Table 3. The calculated values agree with the experimental values so that there are four points for each of these curves. For the curves with unmeasured E(abs) values, there are still three data points, so the calculated values can be obtained from the curves. These follow the predicted systematic variation as shown in Figure 4. Four curves for $I_2(-)$ were adjusted to have a common E(abs) at about 1.68 eV, as shown in Table 3. The S plots make it

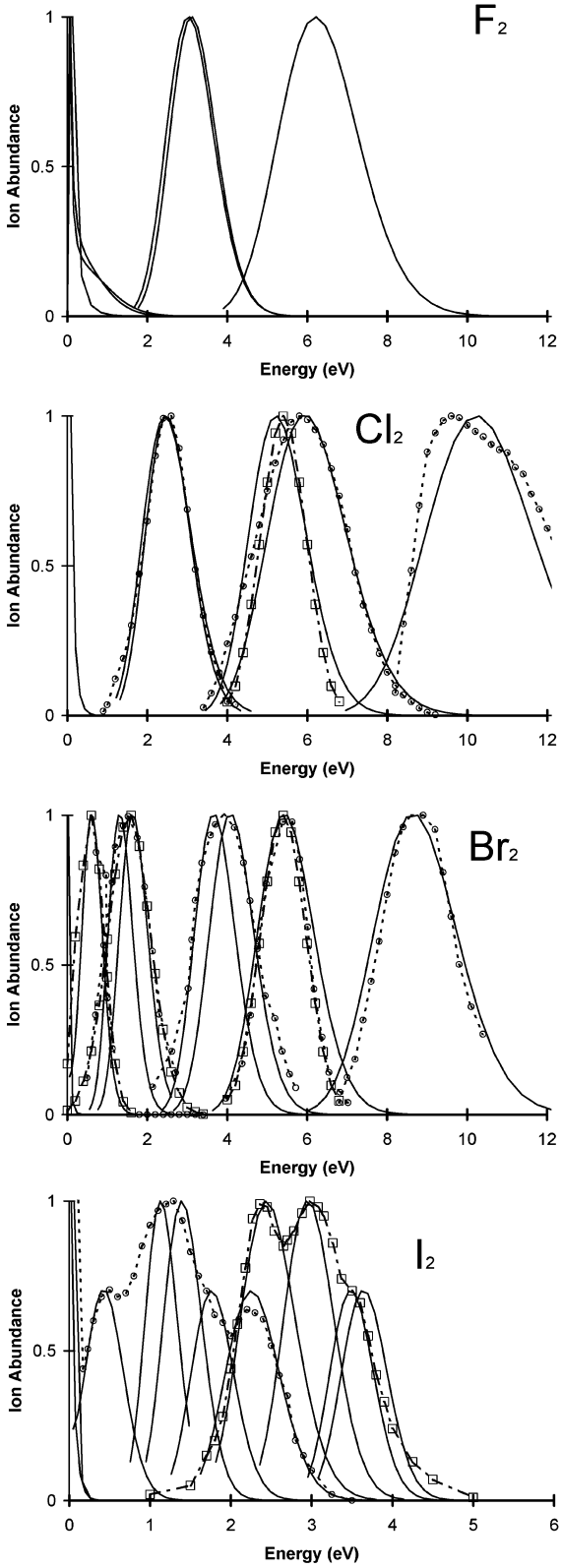

Figure 5. Calculated electron-impact ion distributions for F_2, Cl_2, Br_2, and I_2. Experimental data are shown for all but F_2 (refs 11−14). The energy scale for I_2 is one-half that of the others or 0−6 eV.

easier to visualize this isobestic point for $I_2(-)$ and compare the set of X_2 curves in Figure 6. The E(abs) and the VE_a data are easily observed at the vertical lines shown in each plot. The crossings of the first excited states with the neutral curve agree with the E_1 from the ECD data, which is the fifth point on some of the curves. The excited-state frequencies and internuclear distances are less certain because the two quantities are

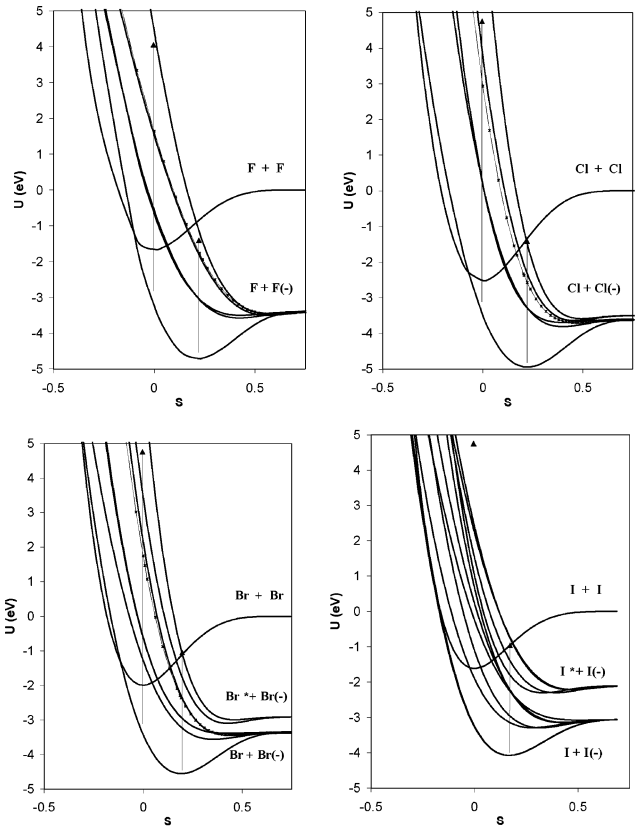

Figure 6. Optimized HIMPEC for $X_2(-)$. Parameters and dimensionless constants are given in Table 3.

correlated. The major changes in these curves are due to the recently reported AMB data for F_2: the new $Ar_2(+)$ data used for $Cl_2(-)$ and the lower experimental dissociation energy measured for the $\Pi_{1/2}$ state of $I_2(-)$, which led to the two new curves for $Br_2(-)$.[6−9]

Anion States of Group VI Homonuclear Diatomics

In 1943, Bates and Massey suggested that the mode of formation of $O_2(-)$ could be established using simple molecular orbital methods.[44] The relative bond order of the ground states of the group VII X_2 and group I M_2 anions is 0.5 since the neutral has two bonding electrons and the ion has a net of one bonding electron. However, all of the experimental bond orders calculated by dividing the bond energy of the anion by that of the neutral are larger than $^1/_2$. The smallest is $^{1.3}/_{2.5} = 0.52$ for $Cl_2(-)$, and the largest is about 1 for $Cs_2(-)$. The predicted relative bond order for the ground state of group VI anions is $^3/_4 = 0.75$. This calculation led to different theoretical estimates of the AE_a of O_2: A$E_a(O_2)$ = AE_a(O) + 0.75$D_0(O_2)$ − $D_0(O_2)$ = AE_a(O) − 1.2 eV. When the E_a of the O atom was believed to be 2.2 eV, this gave 1 eV, in agreement with the Born−Haber value.[17] Later, the E_a of the O atom was determined to be 1.46 eV, which gives a value of 0.26 eV between the ES value, 0.46 ± 0.02 eV, and the PD value, 0.15 ± 0.1 eV.[18,19] When the ES value was confirmed, the 1.07 ± 0.07 eV value determined by several techniques, the 0.15 ± 0.1 eV value, and other values were abandoned because only one state was considered.[5,18,20] With 24 predicted states, all of the experimental values can be explained.[45,46]

In Figure 7, the anionic bond orders relative to that of the ground-state neutral are compared with experimental values for the three lowest states of the neutral, Michels' calculated values, and the present experimental values. The three neutral states

TABLE 3: Morse Parameters and Dimensionless Constants for Neutral and Anionic Morse Potentials of X_2

species		k_A	k_B	k_R	D_o (eV)	r_e (pm)	υ (cm^{-1})	$-VE_a$ (eV)	E(abs) (eV)
F_2	neutral	1.00	1.00	1.00	1.60	141	917		
F_2^-	A $^2\Sigma_u^+$	1.634	0.625	3.372	1.28	180	510	−1.62	
	B $^2\Pi_{g3/2}$	0.555	0.525	2.840	0.170	245	159	1.07	**1.67**
	B $^2\Pi_{g1/2}$	0.390	0.581	2.439	0.095	247	133	0.95	**1.67**
	C $^2\Pi_{u3/2}$	0.379	0.390	3.692	0.060	337	71	3.06	2.88
	C $^2\Pi_{u1/2}$	0.517	0.380	4.011	0.105	322	90	3.14	2.86
	D $^2\Sigma_g^+$	0.430	0.460	5.596	0.050	328	76.8	6.05	3.63
Cl_2	neutral	1.00	1.00	1.00	2.48	199	560		
Cl_2^-	A $^2\Sigma_u^+$	1.082	0.641	2.328	1.31	256	255	−1.01	
	B $^2\Pi_{g3/2}$	0.431	0.638	2.370	0.191	331	101	2.66	**1.64**
	B $^2\Pi_{g1/2}$	0.251	0.780	2.016	0.074	331	78	2.67	**1.64**
	C $^2\Pi_{u3/2}$	0.255	0.613	3.076	0.050	400	50.3	5.32	2.57
	C $^2\Pi_{u1/2}$	0.367	0.624	3.603	0.090	368	68.2	6.19	2.69
	D $^2\Sigma_g^+$	0.419	0.653	5.441	0.077	393	66.3	10.56	**3.47**
Br_2	neutral	1.00	1.00	1.00	1.98	228	323		
Br_2^-	A $^2\Sigma_u^+$	1.180	0.641	2.328	1.180	282	160	−1.45	
	B $^2\Pi_{g3/2}$	0.438	0.598	1.926	0.195	354	61.	0.70	**1.32**
	B $^2\Pi_{g1/2}$	0.134	0.744	1.653	0.020	400	25	1.37	**1.62**
	B $^2\Pi_{g1/2}$	0.147	0.728	1.671	0.024	398	26.7	1.35	**1.62**
	C $^2\Pi_{u3/2}$	0.344	0.628	3.253	0.070	410	38.7	3.72	2.18
	C $^2\Pi_{u3/2}$	0.383	0.632	3.546	0.080	407	41.6	3.72	2.24
	C $^2\Pi_{u1/2}$	0.627	0.651	4.380	0.180	380	63	5.28	2.57
	D $^2\Sigma_g^+$	0.494	0.692	5.875	0.080	410	45.6	8.79	**3.38**
I_2	neutral	1.00	1.00	1.00	1.54	267	215		
I_2^-	A1(1/2)	1.187	0.645	2.242	1.007	320.5	110	−1.67	
	A1(1/2)	1.194	0.651	2.264	1.007	320.5	111	−1.61	
	B1(3/2)	0.491	0.649	1.702	0.225	371	52.5	−0.30	0.87
	B1(3/2)	0.579	0.612	2.372	0.225	392	49.5	0.50	**1.01**
	B1(1/2)	0.125	0.557	1.992	0.012	537	10.6	1.35	**1.68**
	B1(1/2)	0.173	0.601	2.297	0.020	501	14.7	1.69	**1.65**
	C1(3/2)	0.376	0.523	2.789	0.080	475	25.3	1.83	**1.68**
	C1(3/2)	0.383	0.587	3.080	0.075	460	27.5	2.27	**1.69**
	C2(1/2)	0.628	0.654	3.118	0.194	400	50	2.35	**2.11**
	C2(1/2)	0.663	0.524	3.491	0.194	439	40	2.82	2.45
	D2(1/2)	0.501	0.439	3.569	0.108	510	25	3.45	**3.03**
	D2(1/2)	0.509	0.461	3.691	0.108	500	26.3	3.61	**3.03**

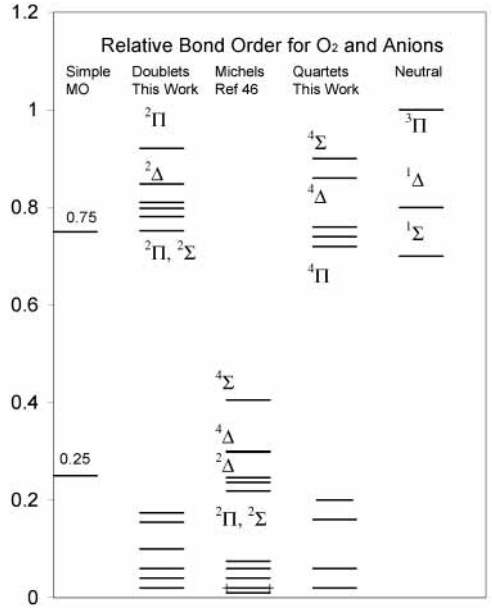

Figure 7. Energy-level diagram for the neutral and for anions of diatomic oxygen expressed as the relative bond order to the ground-state neutral.

have two antibonding and six bonding electrons, giving four net bonding electrons. The 12 M states correspond to the addition of one antibonding electron to the three neutral states, which gives a relative bond order of $^3/_4 = 0.75$. In the 12 D states, a bonding electron is promoted to an antibonding orbital, and the relative bond order is $^1/_4$ or 0.25. The two experimental D curves have relative bond orders of about 0.2. The 11 relative bond orders for the bound states calculated by Michels range from zero to 0.4 as indicated in Figure 7. The 12 unbound curves have a relative bond order of zero. Thus, the calculated dissociation energies are smaller and the internuclear distances are larger than for the experimental D curves.

Theoretical ab initio calculations have reproduced the E_a of 0.430 and 0.450 ± 0.002 eV.[47,48] However, as shown in a review of density functional calculations and experimental PES values, the density functional E_a for O_2 vary from 0.36 to 1.08 eV depending on the functional. Only the BHLYP value is lower than 0.430 ± 0.002 eV. The average of the B3LYP, BLYP, and BP86 values is 0.64 ± 0.01 eV and for the LSDA and B3P86 functionals, the average is 1.07 ± 0.01 eV. These values cover the experimental range but do not support them because all of the density functional E_a for the homonuclear diatomic molecules are larger than the experimental values. The average of the E_a for C_2 from the six above functionals is 3.57 ± 0.12 eV compared to an experimental value of 3.27 ± 0.008 eV.[49]

Massey illustrated four nondetaching states of $O_2(-)$ with three M(2), two M(0), and one D(0) curve. These are Mc(2, 0) since they cross the polarization curve below the lowest limit. The internuclear distances ranged from 140 to 170 pm. Comparable HIMPEC using updated properties and the same E_a, VE_a, and r_e and other curves calculated from experimental data between 1967 and 1999 are shown in Figure 8. These are

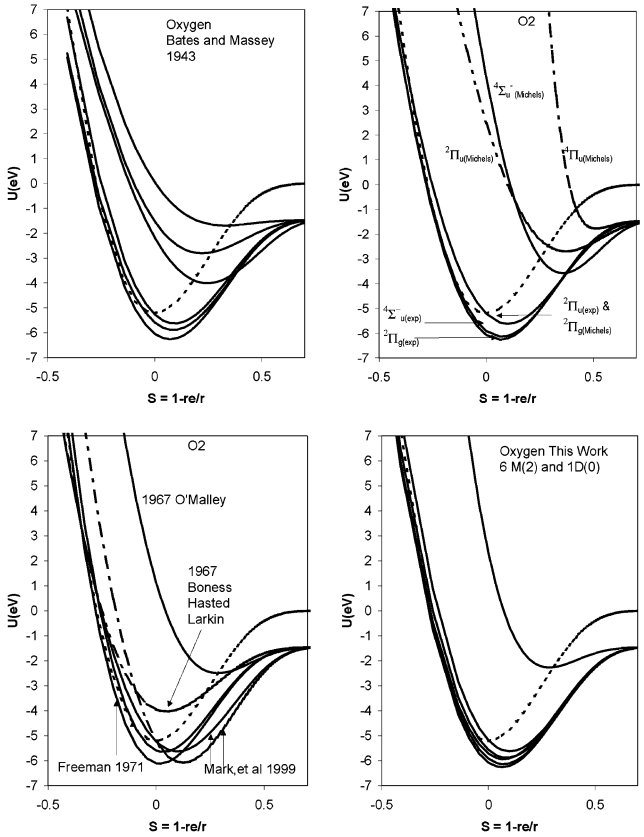

Figure 8. Morse potential energy curves calculated from approximate curves proposed by Bates and Massey,[44] experimental curves from the literature[21,25,30,31] and this study, and theoretical curves by Michels.[46] The BHL 1967 curve is an approximation to a polarization curve.

compared with Michels' $^2\Pi$, $^4\Sigma$, and $^4\Pi$, bound curves, and the previously reported D(0) and the present M(2) curves. The doublet and quartet M and D curves are shown in separate plots in Figure 9.

The PES E_a values of 0.430 and 0.450 ± 0.002 eV are the most precise values for O_2, and the Born−Haber value of 0.9 ± 0.1 eV is the least precise. The ECD values are just as certain since a data reduction procedure cannot degrade the quality. An incidental TCT measurement gives an E_a of O_2 that is greater than 0.8 eV. In the anion mass spectrum of anthracene with a trace amount of O_2 and water, the anthracene$(H_2O)_{1,2,3}$ anions are observed with $O_2(-)$ but not with its hydrates. Thus, $O_2(-)$ was formed by charge transfer from the anions of anthracene with an E_a greater than 0.8 eV.[40] In the PES spectra of $O_2(-)$, small peaks are observed at 0.1, 0.2, 0.3, 0.5, 0.7, 0.75, 0.95, and 1.07 eV. These have been ignored or assigned to "hot" bands of the $^2\Pi_u$ state but coincide with E_a reported by other techniques. If these are due to different electronic states, then they give more precise values from which to construct the Morse curves. The peak widths for the higher E_a indicate that the internuclear distances for these states are between the measured value of the neutral, 121 pm, and that for the $^2\Pi_u$ state, 134 pm. Likewise, the frequencies should be between the two measured frequencies. The M(1) states with the lower E_a have larger internuclear distances and smaller frequencies than the $^2\Pi_u$ state.[24,40]

Michels calculated dissociation energies for $O_2(-)$ ranging from 0 to 2.11 eV for nine bound states.[46] These are D(0) curves since the E_a and VE_a are negative and vertical electron impact leads to dissociation. The experimental E_a for O_2 can be assigned to these states. The VE_a range from 0.9 to − 0.75 eV. The E_1

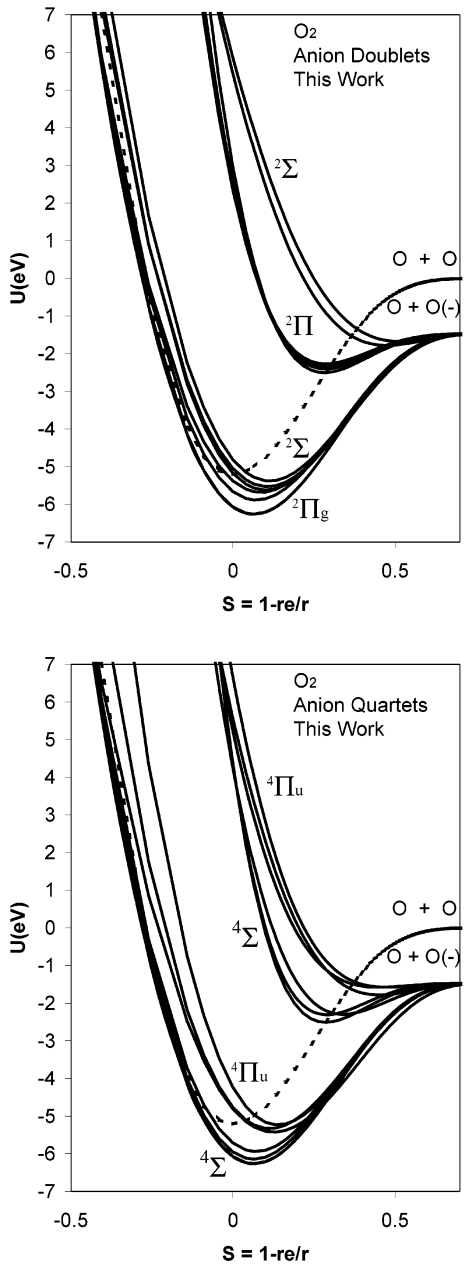

Figure 9. Twenty four HIMPEC for $O_2(-)$. Data and state assignments are given in Tables 4 and 5. Spin−orbit coupling states are not shown.

determined from ECD data range from 0.05 to 1.9 eV. These points and estimated r_e values and frequencies can be used to define six M(2) curves (E_a and VE_a > 0) and six M(1) curves (only E_a > 0). Three quartet states and two doublet states separated by 1 eV are predicted to lie between the ground state and the first excited $^2\Pi_u$ state.[46] The E_a shown in Table 4 were obtained by scaling to this difference. The E_a of the $^4\Sigma_u^-$ state is assigned a value of 0.95 eV, and the $^4\Delta_g$ state and accidentally degenerate $^4\Sigma_g^+$ states are assigned E_a = 0.75 eV, which is 0.2 eV above the $^4\Sigma_u^-$ state. The two doublet states are assigned E_a = 0.7 and 0.5 eV. The other M states are assigned E_a = 0.4_5, 0.3 0.2_2, 0.1_5, and 0.0_5 eV, giving six M(2) and six M(1) states.

The remaining 12 curves are D(0) but are not totally repulsive. The experimental Morse parameters of the $^2\Pi_u$ state give guidance for the other D curves. The states can be assigned to the same order as that of the M states but are highly speculative. The E_a range from −2.6 ± 0.2 to − 3.5 ± 0.1 eV, and since

TABLE 4: Electron Affinities and Activation Energies for O_2 and Morse Parameters for $O_2(-)$

state	D_e (eV)	r_e (pm)	υ_e (cm^{-1})	E_a (eV)	VE_a (eV)	E_1 (eV)
			Quartet States			
$^4\Sigma_u^-$	4.6	129	1250	0.9_5	0.75	0.9
$^4\Delta_g$	4.4	130	1210	0.7_5	0.5	0.8
$^4\Sigma_g^+$	4.4	130	1210	0.7_5	0.5	0.8
$^4\Pi_u$	3.9	138	1000	0.2_5	−0.4	0.2
$^4\Sigma_g^-$	3.8	136	1089	0.1_5	−0.45	0.2
$^4\Pi_g$	3.7	140	1089	0.0_5	−0.9	0.5
$^4\Sigma_u^-$	1	169	700	-2.6_5	−9.5	3.5
$^4\Delta_u$	0.8	183	510	-2.8_5	−9.5	3.5
$^4\Sigma_u^+$	0.8	170	650	-2.8_5	−9.6	3.5
$^4\Pi_u$	0.3	220	260	-3.3_5	$-10._8$	4.
$^4\Sigma_g^-$	0.1	220	190	-3.5_5	$-10._9$	4.
$^4\Pi_g$	0.1	230	180	-3.5_5	$-11._9$	4.
			Doublet States			
$^2\Pi_g$	4.7	129	1250	1.0_7	0.86	1.9
$^2\Delta_u$	4.3_5	130	1200	0.7	0.46	0.8
$^2\Sigma_u^+$	4.1_5	132	1125	0.5	0.17	0.1
$^2\Pi_u(1/2)$	4.1	134	1125	0.45	−0.03	0.05
$^2\Pi_u(3/2)$	4.1	134	1125	0.43	−0.03	0.05
$^2\Sigma_g^+$	4.0_5	135	1089	0.36	−0.16	0.1
$^2\Sigma_u^-$	3.8_5	136	1089	0.3	−0.39	0.2
$^2\Pi_g$	1.0	169	670	-2.6_5	-8.1_6	3.
$^2\Delta_g$	0.9	169	620	-2.7_5	-7.6_5	3.
$^2\Sigma_g^-$	0.82	169	610	-2.8_2	-7.7_7	3.
$^2\Pi_u$	0.77	169	592	-2.8_8	-7.5_5	3.
$^2\Sigma_g^-$	0.3	230	235	-3.3_5	$-10._7$	4.
$^2\Sigma_u^-$	0.2	250	180	-3.1_5	$-11._1$	4.

$E_a = E_{dea} + D_0 \pm 0.1$ eV, this gives dissociation energies of 1 to 0.1 eV. The observed $-VE_a$ from electron impact, scattering, or dissociative electron attachment are 0.2, 1, 7.8, and up to 11.9 eV. The observed gas-phase electron-impact data can be modeled using only one upper negative-ion state. The gap between the VE_a of $(7 - 1) = 6$ eV is the splitting of the states at the internuclear distance of the neutral.[26−32] This has been confirmed by dissociative electron attachment to the excited state of the neutral where the peak in the O(−) distribution is shifted by about 1 eV, which is the excitation energy of the neutral. In addition, a second excited state dissociating to the next highest limit is identified about 2 eV higher. Thus, the 12 D peaks leading to the lowest limit should have $-VE_a$ values in the range of 7 to 12 eV. The lowest state in the Franck−Condon region is assigned to the $^2\Pi_u$ state, but several states are assigned larger dissociation energies. These cross this state at larger internuclear distances and give similar VE_a. Better electron-impact data and assignments can improve the D curves.

There are many fewer data for the negative-ion states of S_2, Se_2, and Te_2. Several photoelectron spectra have been obtained for S_2. The most recent has the highest resolution.[34−37] The relative bond orders for the remaining group VI homonuclear diatomic molecules are larger than that for $O_2(-)$. The dimensionless constants for all of the ground states are very similar to those for $O_2(-)$. The $^2\Pi_u$ anionic states characterized by electronic spectra for the higher members of the group VI family are M states. These are M(0) for $S_2(-)$ and $Se_2(-)$, but the curve for $Te_2(-)$ is M(2) because the E_a is positive and it crosses the neutral in the inverted Marcus region. The dimensionless constants are different from those for $O_2(-)$. In addition, their relative bond orders are different on going from about 0.2 in O_2 to 0.6 in Te_2. This increase mirrors that for the ground state since the relative bond orders for $Se_2(-)$ and $Te_2(-)$ are approximately 1 whereas that for $O_2(-)$ is about 0.85. There should be as many states for the isoelectronic ions as for $O_2(-)$. The consistency of the dimensionless constants for the ground-state curves supports the isoelectronic principle, but the differences in the values for the upper state do not justify the use of the $O_2(-)$ parameters. Since there are no other data, only two curves are calculated. These are compared to the 24 curves for $O_2(-)$ in Figure 10. The parameters for the curves are given in Table 5.

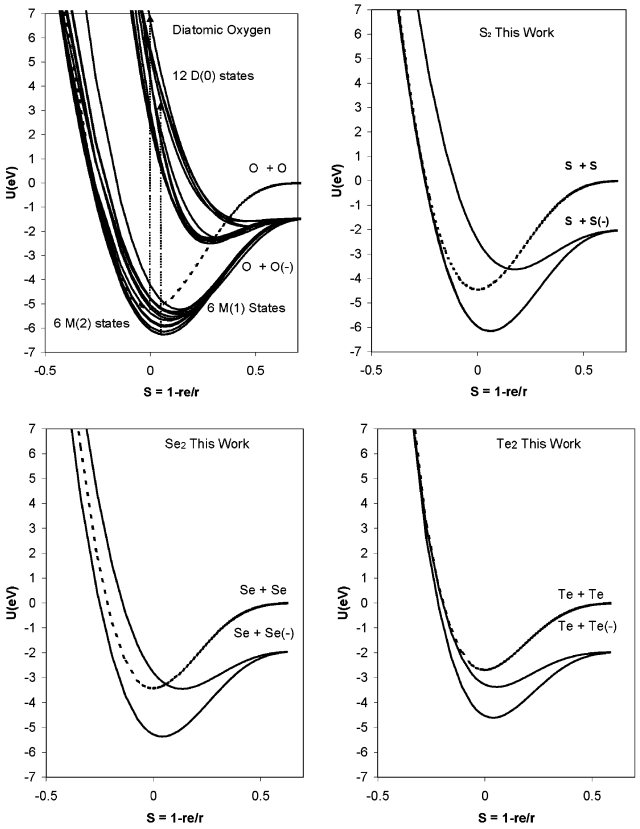

Figure 10. Morse potential energy curves for the neutral and for two anionic states of S_2, Se_2, and Te_2 and the 12 M(2,1) and 12 D(0) for $O_2(-)$.

Conclusions

The Herschbach classification of XY(−) potential energy curves based on molecular ion formation, M, and dissociation, D, in a vertical transition has been used to consolidate the available experimental data systematically to obtain optimum sets of Morse potential energy curves for $X_2(-)$ and $O_2(-)$. The comparison of isoelectronic species and the iterative optimization was simplified by plotting with $S = 1 - (r/r_e)$, the modified Simons−Parr−Finlan reduced distance variable.

A reanalysis of ECD data for Cl_2, Br_2, and I_2 gives two activation energies for thermal electron attachment, E_1. Six curves for F_2 (−) and $Cl_2(-)$, 8 curves for $Br_2(-)$, and 12 curves for $I_2(-)$ were determined from experimental data. The AE_a obtained from $D_0(X_2(-)) = D_0(Rg_2(+))$ and the thermodynamic cycle $AE_a(X_2) = D_0(X_2(-)) + AE_a(X) - D_0(X_2)$ agree with the measured values and except for I_2 are more precise: F_2, 3.08; Cl_2, 2.45; Br_2, 2.56; and I_2, 2.50 (±0.02 eV). New experimental bond-dissociation energies for $Ar_2(+)$ were used for all of the states of $Cl_2(-)$. The $^2\Pi_g(1/2)$ curves for $I_2(-)$ and $Br_2(-)$ were calculated using a lower dissociation energy (0.02 eV) that was measured for the $I_2(-)$ but not observed in the $Xe_2(+)$ spectra. On the basis of the isoelectronic principle, there should be similar curves for $Kr_2(+)$ and $Xe_2(+)$.

New ECD data for $O_2(-)$ confirm previously observed E_a and define new E_1. Peaks observed in high-resolution PES for $O_2(-)$ are assigned to negative-ion states on the basis of

TABLE 5: Morse Parameters and Dimensionless Constants for Neutrals and Anions of Group VI Homonuclear Diatomic Molecules

species		D_o (eV)	r_e (pm)	v (cm^{-1})	k_A	k_B	k_R
O_2	neutral	5.11	121	1580	1.000	1.000	1.000
$O_2(-)$	$^4\Sigma_u^-$	4.6	129	1250	1.080	0.835	1.298
	$^4\Delta_g$	4.4	130	1210	1.054	0.826	1.292
	$^4\Sigma_g^+$	4.4	130	1210	1.054	0.826	1.292
	$^4\Pi_u$	3.9	138	1000	1.062	0.726	1.482
	$^4\Sigma_g^-$	3.8	136	1089	1.028	0.800	1.422
	$^4\Pi_g$	3.7	140	1089	1.096	0.810	1.660
	$^4\Sigma_u^-$	1	169	700	0.713	0.990	2.537
	$^4\Delta_u$	0.8	183	510	0.608	0.808	2.311
	$^4\Sigma_g^-$	0.8	170	650	0.617	1.024	2.356
	$^4\Pi_u$	0.3	220	260	0.353	0.668	2.055
	$^4\Sigma_g^-$	0.1	220	190	0.189	0.825	1.664
	$^4\Pi_g$	0.1	230	180	0.205	0.780	1.972
	$^2\Pi_g$	4.7	129	1250	1.105	0.824	1.325
	$^2\Delta_u$	4.3_5	130	1200	1.041	0.824	1.276
	$^2\Sigma_u^+$	4.1_5	132	1125	1.027	0.791	1.302
	$^2\Pi_u(1/2)$	4.0_7	134	1125	1.057	0.798	1.404
	$^2\Pi_u(3/2)$	4.1_0	134	1125	1.062	0.796	1.409
	$^2\Sigma_g^+$	4.0_5	135	1089	1.050	0.780	1.412
	$^2\Sigma_u^-$	3.8_5	136	1089	1.039	0.795	1.435
	$^2\Pi_g$	1.0	169	670	0.675	0.948	2.276
	$^2\Delta_g$	0.9	169	620	0.582	0.940	1.942
	$^2\Sigma_u^-$	0.82	169	610	0.558	0.951	1.890
	$^2\Pi_u$	0.77	169	592	0.525	0.952	1.780
	$^2\Sigma_g^-$	0.3	230	235	0.350	0.605	2.026
	$^2\Sigma_u^-$	0.2	250	180	0.283	0.566	1.973
S_2	neutral	4.46	190	726	1.000	1.000	1.000
$S_2(-)$	$^2\Pi_g$	4.11	202	601	1.128	0.858	1.367
	$^2\Pi_u$	1.60	230	364	0.677	0.831	1.258
Se_2	neutral	3.44	217	387	1.000	1.000	1.000
$Se_2(-)$	$^2\Pi_g$	3.43	226	330	1.153	0.853	1.331
	$^2\Pi_u$	1.50	250	217	0.730	0.845	1.210
Te_2	neutral	2.69	256	247	1.000	1.000	1.000
$Te_2(-)$	$^2\Pi_g$	2.63	266	223	1.141	0.911	1.325
	$^2\Pi_u$	1.40	270	180	0.661	1.007	0.833

published E_a. Twelve M and 12 D HIMPEC have been constructed for $O_2(-)$. This is an example of the synergism between theoretical models and experimental data since 24 low-lying states of the superoxide anion were predicted nearly 40 years ago whereas the assignment of the experimental data to those states is a result of this paper. Just as O_2 is unique in having three low-lying bound states, so also is $O_2(-)$ unique in having so many low-lying bound states. Two anion curves are presented for S_2, Se_2, and Te_2. As stated by Mulliken in offering curves for I_2 in 1971, "While the curves shown cannot possibly be quantitatively correct, they should be useful as forming a sort of zeroth approximation to the true curves." [50]

Acknowledgment. We thank the reviewers for their constructive suggestions.

References and Notes

(1) Chen, E. S.; Chen, E. C. M. *J. Phys. Chem. A* **2002**, *106*, 6665.
(2) Chen, E. S.; Chen, E. C. M. *Chem. Phys Lett.* **1998**, *491*, 293.
(3) Herschbach, D. R. *Adv. Chem. Phys.* **1966**, *10*, 250.
(4) Parr, R. G.; Ayres, P. W. *J. Phys. Chem. A* **2002**, *106*, 5060.
(5) Christodoulides, A. A.; McCorkle, D. L.; Christophorou, L. G. Electron Affinities of Atoms, Molecules and Radicals. In *Electron−Molecule Interactions and their Applications;* Academic Press: New York, 1984. National Institute of Standards and Technology (NIST) Chemistry WebBook. http://webbook.nist.gov/ (accessed 2001).
(6) Zanni, M. T.; Taylor, T. R.; Greenblatt, B. J.; Miller, W. H.; Neumark, D. M. *J. Chem. Phys.* **1997**, *107*, 7613.
(7) Kleyn, A. W.; Moutinho, A. M. C. *J. Phys. B: At. Mol. Opt. Phys.* **2001**, *34*, R1.
(8) Zanni, M. T.; Batista, V. S.; Greenblatt, B. J.; Soep, B.; Neumark, D. M. *J. Chem. Phys.* **1999**, *110*, 3748.
(9) Rupper, P.; Merkt, F. *J. Chem. Phys.* **2002**, *117*, 4264.
(10) Chen, E. C. M.; Wentworth, W. E. *J. Phys. Chem.* **1985**, *89*, 4099.
(11) Kurepa, M. V.; Babic, D. S.; Belic, D. S. *J. Phys. B: At. Mol. Opt. Phys.* **1978**, *11*, 3719.
(12) Kurepa, M. V.; Babic, D. S.; Belic, D. S. *J. Phys. B: At. Mol. Opt. Phys.* **1981**, *14*, 375.
(13) Azria, R.; Abouaf, R.; Tellet-Billy, D. *J. Phys. B: At. Mol. Opt. Phys.* **1982**, *16*, L569.
(14) Azria, R.; Abouaf, R.; Tellet-Billy, D. *J. Phys. B: At. Mol. Opt. Phys.* **1988**, *21*, L213.
(15) Ayala, J. A.; Chen, E. C. M.; Wentworth, W. E. *J. Phys. Chem.* **1981**, *85*, 768.
(16) Caledonia, G. E. *Chem. Rev.* **1975**, 75, 333.
(17) Pritchard, H. O. *Chem. Rev.* **1953**, *52*, 529.
(18) Burch, D. S.; Smith, S. J.; Branscomb L. M. *Phys. Rev.* **1958**, *112*, 171.
(19) Pack J. L.; Phelps, V. *Phys. Rev. Lett.* **1961**, *6*, 111.
(20) Vogt, D.; Hauffe, B.; Neuert, H. *Z. Phys.* **1970**, *232*, 439.
(21) Freeman, R. R. Ph.D. Dissertation, University of Houston, Houston, TX, 1971.
(22) Chen, E. S.; Wentworth, W. E.; Chen, E. C. M. *J. Mol. Struct.* **2002**, *606*, 1.
(23) Van de Wiel, H. J.; Tommasen, H. *J. Chromatogr.* **1972**, *71*, 1.
(24) Schiedt, J.; Weinkauf, R. *Z. Naturforsch., A: Phys. Sci.* **1995**, *50*, 1041.
(25) Matejcik, S.; Stampfli, P.; Stamatovic, A.; Scheier, P.; Mark, T. D. *J. Chem. Phys.* **1999**, *111*, 3548.
(26) Bailey, C. J.; Lavrich, D. J.; Serxner, D.; Johnson, M. A. *J. Chem. Phys.* **1996**, *105*, 1807.
(27) Sambe, H.; Ramaker, D. E. *Phys. Rev. A: At., Mol., Opt. Phys.* **1989**, *40*, 3651.
(28) Bass, A. D.; Parenteau, L.; Weik, F.; Sanche, L. *J. Chem. Phys* **2001**, *115*, 4811.
(29) Jaffke, T.; Meinke, M.; Hashemi, R.; Christophorou, L. G.; Illenberger, E. *Chem. Phys Lett.* **1992**, *193*, 62.
(30) O'Malley, T. F. *Phys. Rev. A: At., Mol., Opt. Phys.* **1966**, *150*, 14.
(31) Boness, M. J. W.; Hasted, J. B.; Larkin, I. W. *Proc. R. Soc. London, Ser. A* **1968**, *305*, 493.
(32) Ferguson, E. E. *Advances in Electronic and Electron Physics*; Academic Press: New York, 1968; p 1.
(33) Lind, J.; Shen, X.; Merenyi, G. and Johnsson, B. O. *J. Am. Chem. Soc.* **1989**, *111*, 7654.
(34) Snodgrass, J. T.; Coe, J. V.; McHugh, K. M.; Friedhoff, C. B.; Bowen, K. H. *J. Phys. Chem.* **1989**, *93*, 1249.
(35) Celotta, R. J.; Bennett, R. A.; Hall, J. L. *J. Chem Phys.* **1986**, *60*, 1740.
(36) Hunsicker, S.; Jones, R. O.; Gantefor, G. *J. Chem. Phys.* **1995**, *102*, 5917.
(37) Moran, N. R.; Ellison, G. B. *J. Phys. Chem.* **1988**, *92*, 1794.
(38) Chen, E. C. M.; Wentworth, W. E.; Carr, S.; Chen, E. S. *J. Chromatogr., A* **1998**, *827*, 91.
(39) Lyons, L. E.; Morris, G. C.; Warren, L. J. *J. Phys. Chem.* **1968**, *72*, 3677.
(40) Chen, E. C. M.; Chen, E. S. *J. Chromatogr., A* **2002**, *952*, 173.
(41) Wiley, J. R.; Chen, E. C. M.; Wentworth, W. E. *J. Phys. Chem.* **1993**, *97*, 1256.
(42) Chen, E. C. M.; Wiley, J. R.; Batten, C. F.; Wentworth, W. E. *J. Phys. Chem.* **1994**, *98*, 88.
(43) Stemmler, E. A.; Hites, R. A. *Electron Capture Negative Ion Mass Spectra of Environmental Contaminants and Related Compounds*; VCH: New York, 1988.
(44) Bates, D. R.; Massey, H. S. W. *Proc. R. Soc. London, Ser. A* **1943**, *239*, 33.
(45) Gilmore, F. R. *J. Quant. Spectrosc. Radiat. Transfer* **1965**, *5*, 369.
(46) Michels, H. H. *Adv. Chem. Phys.* **1981**, *45*, 227.
(47) Sordo, J. A. *J. Chem. Phys.* **2001**, *114*, 1974.
(48) Neogrady, P.; Medved, M.; Cernusak, I.; Urban, M. *Mol. Phys.* **2002**, *100*, 541.
(49) Reinstra-Kiracofe, J. C.; Tschumper, G. S.; Schaefer, H. F.; Nandi, S.; Ellison, G. B. *Chem. Rev.* **2002**, *102*, 231.
(50) Mulliken, R. S. *J. Chem. Phys.* **1971**, *55*, 28.